Mechanical Properties of Carbon Nanotubes Using Molecular Dynamics Simulations with the Inlayer van der Waals Interactions

W.H. Chen[1], H.C. Cheng[2] and Y.C. Hsu[3]

Abstract: The evaluation of the fundamental mechanical properties of single/multi-walled carbon nanotubes(S/MWCNTs) is of great importance for their industrial applications. The present work is thus devoted to the determination of various mechanical properties of S/MWCNTs using molecular dynamics (MD) simulations. The study first focuses on the exploration of the effect of the weak inlayer van der Waals (vdW) atomistic interactions on the mechanical properties of S/MWCNTs. Secondly, in addition to the zig-zag and armchair types of CNTs, the hybrid type of MWCNTs that comprise a zig-zag outer tube and an inner armchair tube is also analyzed. Thirdly, the investigation is extended to deal with the influence of the axial orientation mismatch between the inner and outer layers of MWCNTs on the associated mechanical properties. Lastly, the behaviors of the interlayer shear force/strength of MWCNTs are discussed in detail.

In the MD simulations, the force field between two carbon atoms is modeled with the Tersoff-Brenner (TB) potential while the inlayer/interlayer vdW atomistic interactions are simulated with the Lennard-Jones (L-J) potential. The effectiveness of the MD simulations is demonstrated by comparing the computed results with the theoretical/experimental data available in literature.

Some interesting and essential results are presented. With different dimensions and geometries of CNTs, the inlayer vdW atomistic interactions can have up to about 9% increase of the elastic moduli, 27% decrease of the Poisson's ratios, 12% growth of the shear moduli, and 13% enhancement of the interlayer shear strength. The mechanical properties of the hybrid MWCNTs are found to be midway between the zig-zag and armchair MWCNTs. It is also detected that the axial orientation mismatch between the inner and outer layers of a double-walled CNT has a trivial impact on the mechanical properties of CNTs. To separate the inner layer of a double-walled CNT from its outer layer, it requires a minimum external force of 0.889nN for the zig-zag type, 0.550 nN for hybrid type and 0.493nN for the armchair type.

In summary, the effect of the inlayer vdW atomistic interactions can not be neglected and should receive attention in the MD simulations of the mechanical properties of CNTs.

Keyword: Molecular Dynamics Simulation, Carbon Nanotubes, Inlayer van der Waals Force, Mechanical Properties.

1 Introduction

Ever since the exciting discovery of carbon nanotubes (CNTs) (Iijima, 1991), an explosive growth in finding novel nano-structured materials with advanced material properties has been stimulated in material science. Mainly due to their exceptionally remarkable mechanical, electrical and thermal properties and presumed minor defects, which have never been seen before, CNTs present a great potential for a wide range of applications from such as fiber-reinforcement composites, nanoelectronics, drug delivery to field

---

[1] Tsing Hua Chair Professor, Department of Power Mechanical Engineering, National Tsing Hua University, Hsinchu, Taiwan 30013, R.O.C., whchen@pme.nthu.edu.tw

[2] Professor, Department of Aerospace and Systems Engineering, Feng Chia University, Taichung, Taiwan 40724, R.O.C., hccheng@fcu.edu.tw

[3] Graduate Student, Department of Power Mechanical Engineering, National Tsing Hua University, Hsinchu, Taiwan 30013, R.O.C.

emission panel display or electromechanical sensors(Maiti, 2002) etc. Moreover, their nano-dimensions have made them particularly ideal for serving as a link between continuum behaviors and atomistic responses.

If tiny CNTs are to be further used in industrial applications, such as nanocomposites, their basic mechanical properties must be identified. Presently, a great deal of research work is underway. However, researches in processing, characterization and modeling of CNTs remain challenging due to that they retain diversified electrical, thermal, and structural properties that change with their diameter, length, and chirality. Wei et al. (2002) discussed the temperature-dependent, plastic collapse of SWCNTs under axial compression by MD simulation; Ling and Atluri (2006) investigated the thermal capacity and expansion of SWCNTs using lattice-based cell model. Over the past few years, many new measurement tools and nano-manipulation techniques have been developed, including some indispensable, high-resolution microscopes, such as transmission electron microscope (TEM) and scanning probe microscope (SPM). The development has resulted in an extensive study on experimental characterization of the mechanical properties of CNTs. For example, Treacy et al. (1996) assessed the Young's modulus of a set of cantilevered MWCNTs subjected to thermal vibration based on the free-end amplitude measured by TEM and Wong et al. (1997) measured the deflection of CNTs through an atomistic force microscope (AFM)-based technique to predict the bending modulus. Others can be seen also in Falvo et al. (1997), Lourie and Wagner (1998), Krishnan et al (1998), Poncharal et al. (1999) and Yu et al. (2000). However, there are some limitations of the experimental approaches. For instance, there is no assurance of the structural perfection of the CNT specimens used in the experimental measurements, leading to the uncertainty of the results. In addition, they become more and more cost-ineffective and technically challenging as the dimension of the nano-structures to be measured gets smaller and smaller. Most importantly, they could not provide a detailed insight of the physical behaviors of nano-materials.

Computational approaches are, on the other hand, more cost-effective and efficient, and hence, become a significant and powerful tool in the design and analysis of nano-materials nowadays, in which the classical molecular dynamics simulations, and multi-temporal and spatial scale simulations are extremely applied in the analysis of nanomechanics. (see, e.g. Shen and Atluri, 2004a). In literature, several empirical potential functions have been introduced for carbon or silicon atoms with covalent bonds, and have achieved great success in many aspects. By the approach, many previous works can be found in the context of characterization of mechanical properties of CNTs. For example, Lu (1997) estimated the Young's modulus and Poisson's ratio of S/MWCNTs based on an empirical force-constant model; Hernandez et al. (1998) calculated the Young's modulus of single-walled carbon and $B_xC_yN_z$ nanotubes based on nonorthogonal tight-binding formalism; Gao et al. (1998) investigated the mechanical and vibrational properties of SWCNTs based on MD simulation; Lier et al. (2000) applied the ab initio method to calculate the Young's modulus and Poisson's ratio of SWCNTs; Nasdala et al. (2005) presented that the failure mechanism of SWCNTs depends on the location and number of defects by finite element analysis; and Xie and Long (2006) investigated the fundamental frequencies for the cantilever single-walled and double-walled carbon nanotube by micropolar mechanics etc. Among the existing computational techniques, despite that more accurate solutions can be provided by the ab initio methods, the MD approaches are generally preferred in nanotechnology due to their less intensive computational effort. In addition, MD simulation is particularly suitable for use in the characterization of the mechanical properties of CNTs because of the neglect of the motion of electrons in the modeling.

In recent years, several studies were carried out on the interlayer vdW atomistic interactions in MWCNTs. For example, Li and Chou (2003a) discussed their influence on the mechanical properties of MWCNTs; and Guo and Gao (2005) investigated the interlayer shear strength due to in-

terlayer vdW atomistic interactions of MWCNTs through relative, interlayer motion between two neighboring layers. However, these studies by no means took into account the effect of the in-layer vdW interactions of pair atoms. According to the classical molecular mechanics (Burkert and Allinger, 1982), simple molecular mechanics force fields include bond stretching, angle bending, torsion, and non-bonding interactions in their make-up. As a result, except the bonding interactions, the non-bonding forces shall also contribute to the vdW atomistic interactions in principle. Based on the usual convention of molecular mechanics (Wiberg, 1965; Rappe and Casewit, 1997), the weak non-bonding vdW interactions between two atoms that are apart less than or equal to two bonds should be excluded due to that they have been implicitly included in any empirical interatomistic potential energy. This also implies that those other than that shall be considered. Thus, the underlying objective of the study attempts to explore the dependence of the in-layer vdW atomistic interactions on the mechanical properties of various S/MWCNTs through MD simulations. To describe the covalent bonds in CNTs, the Tersoff-Brenner potential (Brenner, 1990) is applied in this study. It should be however noted that the non-bonding interactions, such as van der Waals forces, were not considered in the potential function (see, Brenner, 1990). In the investigation, the MWCNTs with a hybrid helicity across different layers are also addressed, in addition to the zig-zag and armchair types of S/MWCNTs. The mechanical properties of S/MWCNTs under investigation include the elastic modulus, Poisson's ratio, shear modulus and the interlayer shear strength of MWCNTs. The effects of sizes, such as the radius and length of MWCNTs, and the interlayer spacing on the interlayer shear strength are evaluated. The modeling results are extensively compared against the published data in literature through either MD simulations or experimental studies. In principal, the new contribution of the present study includes the investigation of the effects of the weak inlayer vdW atomistic interactions and the orientation variation between the inner and outer layers of MWCNTs on the associated mechan-

ical behaviors, the exploration of the interlayer shear strength of MWCNTs, and the investigation of the mechanical properties of various types of MWCNTs. In addition, some new findings of the thermal-mechanical behaviors of CNTs are presented.

2 Molecular Structures of CNTs

A CNT structure can be considered as a result of a number of rolled-up graphene sheets. Accordingly, the bonding structure between carbon atoms in a CNT system is similar to that of graphite. CNTs can be either metallic or semi-conducting depending on their chirality. The chirality mainly determines the density, lattice structure, material strength, and conductance of CNTs. The atomistic bonds basically establish the mechanical properties of CNTs. In a graphene, sp^2 hybridization takes place, in which one s-orbital and two p-orbitals are combined to form three hybrid, in-plane sp^2 bonds, termed as σ-bonds. Each of which is separated by an angle of $120°$. The σ-bond is a very strong covalent bond, resulting in high strength and stiffness along the axis of CNTs. On the other hand, π-bonds resulting from the remaining p-orbital that is in-plane perpendicular to those σ-bonds are relatively weak as compared to σ-bonds. Accordingly, the π-bonds have nothing to do with the out-of-plane interlayer atmoistic interaction, in which it is described by the vdW interaction.

CNTs can be fabricated by way of several synthesis methods, including laser ablation, chemical vapor deposition, and carbon evaporation by arc current discharge etc. The ways of synthesis can significantly influence the mechanical properties of CNTs. In addition, it is worth emphasizing that at the nano-scale, defects are presumably less in CNTs; hence, the strength of CNTs can attain a theoretical limit. In the study, a layered thickness of 3.4 $\mathring{A}$ and an interlayer spacing of 3.4 $\mathring{A}$, which is close to the interlayer separation of graphite, i.e., 3.35 $\mathring{A}$, are assumed for the nanotubes applied. However, it was pointed out by Kiang et al. (1998) that the increased repulsive force resulting from high curvature in consequence of the varied diameter and number of nested layers in

MWCNTs could alter the interlayer spacing. Basically, it increases slightly with the decrease of the CNTs' diameter. It should be noted that the definition of the thickness, the interlayer spacing and the mechanical properties of CNTs, such as elastic modulus and Poisson ratio, would be fundamentally sound only under the continuum assumption.

Based on the continuum assumption, the axial elastic modulus of CNTs can be derived through an axial tension method. When a structure is subjected to an axial deformation, the variation of total potential energy (E) due to the tensile strain (ε) can be represented as the strain energy. As a result, the axial elastic modulus (Y) of the structure can be calculated from the second derivatives of the strain energy density with respect to various strains (Huntington, 1958):

$$Y = -\frac{1}{V_0}\frac{\partial^2 E}{\partial \varepsilon^2}. \tag{1}$$

The total volume of the structure can be defined as the product of the cross-sectional area (A) and the length (L) of the structure. The cross-sectional area of MWCNTs is defined as (Li and Chou, 2003a),

$$A = \pi \left[(R_{outer} + 0.17)^2 - (R_{inner} - 0.17)^2 \right], \tag{2}$$

where R_{outer} stands for the radius of the outermost tube, R_{inner} the radius of the innermost tube, and 0.17 (nm) a half layered thickness of CNTs. For SWCNTs, R_{outer} is equal to R_{inner} and the cross-sectional area A is defined as,

$$A = 2\pi R \times 0.34 (\text{nm})^2.$$

Similarly, the shear modulus of CNTs can be found by a torsion method. While a small angle of twist is applied on one side of CNTs, the variation of total potential energy (E) due to the shear strain (γ) could be observed. According to those results, the shear modulus of CNTs can be presented similarly as (Huntington, 1958):

$$G = -\frac{1}{V_0}\frac{\partial^2 E}{\partial \gamma^2}, \tag{3}$$

The other concerned "continuum" mechanical property for CNTs is the Poisson's ratio. The ratio defines the absolute value of the ratio of the lateral strain (ε_l) over the axial strain (ε_a), which is defined as:

$$\upsilon = \left| \frac{\varepsilon_l}{\varepsilon_a} \right|. \tag{4}$$

Note that the strain is defined as the deformation per unit length. The Poisson's ratio can be estimated by minimizing the strain energy with respect to both the radial compression and the axial extension.

3 Classical Molecular Dynamics

In principle, molecular dynamics (MD) deals with particle dynamics based on the Newton's second law, and is thus termed as a particle method. The atomistic interactions or bonding mechanisms are described based on certain analytical or empirical potential functions (see, e.g., Stillinger and Weber, 1985; Abell, 1985; Tersoff, 1988; Brenner, 1990; Nordlund et al., 1996), and the formulation of MD is then defined by assessing the spatial gradient of the specified potential function. Extensive reviews on the subject of classical MD simulation are available (Khor and Das Sarma, 1988; Heggie, 1991; Chelikowsky, 1992).

In the investigation, to describe the covalent bonds, i.e., σ-bonds, of carbon atoms, the Tersoff-Brenner potential (Brenner, 1990; Maruyama, 2000) is adopted, which is widely used for studying fullerene and CNTs. In the analysis of MWCNT systems, surface interactions due to π bonds could not be neglected at the scale even though it is relatively weak in comparison with the covalent bonds, σ bonds. An adequate definition of interactions among nested individual layers remains an important challenge for the modeling. In literature, two main empirical models are available for describing interlayer atomistic interactions: (1) the inverse power model and (2) the Morse function model. For instance, Lennard-Jones (1924) proposed a well-known inverse power model, termed as the L-J potential, and Wang et al. (1991) introduced a Morse-type potential for carbon atom systems based on local density approximation. There are pros and cons on these two models. As indicated by Qian et al. (2001), the local density approximation yields a

considerably lower binding energy in the attractive zone while the L-J potential presents a considerably higher atomistic force in the repulsive zone. The deduction is also supported by experimental data. It was thus suggested by Qian et al. (2001) that the local density approximation is preferred as the inter-atomistic distance is less than 3.4 $\mathring{A}$, and the L-J potential as it is greater than 3.4 $\mathring{A}$. The interlayer spacing within MWCNTs is roughly 3.4 $\mathring{A}$, implying that the distance between any two carbon atoms located at two different layers of MWCNTs is equal to or greater than 3.4 $\mathring{A}$. As a result, the L-J potential is used in the investigation to model the interlayer vdW atomistic interactions. In addition to the interlayer ones, the vdW atomistic interactions between any two atoms that are within the same layer but apart beyond two bonds (Rappe and Casewit, 1997) are taken into account. Their effect on the mechanical properties of CNTs is accordingly addressed. Correspondingly, they are also modeled with the L-J potential for the vdW atomistic interactions.

The uniqueness of the current MD simulation can be observed in its integration of two types of potentials, the Tersoff-Brenner and L-J potentials, for simultaneously modeling the covalent bonds between any two adjacent carbon atoms and the vdW atomistic interactions between two atoms that are across layers or in a layer but apart beyond two covalent bonds, respectively. With those two types of interactions, the summarized potential is expressed as:

$$E = \sum_{i}\sum_{j>i}(E_{cov}+E_{vdw}),\qquad(5)$$

where E_{cov} is the covalent bonding energy modeled with Tersoff-Brenner potential (Brenner, 1990; Maruyama, 2000) and E_{vdw} the L-J potential. The total covalent potential of a system is denoted as the sum of individual covalent bond energy:

$$E_{cov} = f_c(r_{ij})\left\{V_R(r_{ij})-b_{ij}V_A(r_{ij})\right\},\qquad(6)$$

where r_{ij} is the distance between two joining atoms, i and j as shown in Fig.1. In order to facilitate the computation of equilibrium of atoms in a CNT system, a specific cutoff function $f_c(r_{ij})$ is embedded in the Tersoff-Brenner potential (Brenner, 1990). Basically, the cutoff function is a simple decaying function that shows the weighting of covalent bonds under some distance and varies from 0 to 1. In Eq. (6), $V_R(r_{ij})$ and $V_A(r_{ij})$ represent the repulsive and attractive interactions, respectively, and b_{ij} denotes the modification of the covalent bonding energy depending on θ_{jik} representing the bonding angle between bonds $i-j$ and bonds $i-k$, as shown in Fig. 1. The detail form of the Tersoff-Brenner potential function and the associated parameters could be found in the reference (Brenner, 1990). The Tersoff-Brenner potential versus distance r_{ij} with different bonding angle θ_{jik} is illustrated in Fig. 2. According to Brenner (1990), the non-bonding interactions such as van der Waals forces were not considered in the potential form.

For a MWCNT, the atomistic interactions across layers are modeled with the vdW potential. The inlayer vdW atomistic interactions are accounted for only when those two atoms are separated beyond two bonds, based on the convention of molecular mechanics (Rappe and Casewit, 1997). Since atom J, K, M and N are less than two bonds apart from atom I, as shown in Fig. 3, they are not modeled with the inlayer vdW interactions. On the other hand, since atom L, O, P and Q consist of a separate distance of more than two bonds from atom I, they are modeled with the vdW atomistic interactions. In the study, the vdW atomistic interactions are characterized by the L-J 12-6 potential (Lennard-Jones, 1924; Battezzatti et al., 1975),

$$E_{vdw}(r_{ij}) = 4\varepsilon\left[\left(\frac{r_0}{r_{ij}}\right)^{12}-\left(\frac{r_0}{r_{ij}}\right)^{6}\right],\qquad(7)$$

where ε is the energy at the minimum in E_{vdw} and r_0 is the distance between two atoms at which E_{vdw} is zero. For carbon atoms, $\varepsilon = 0.0556$ *kcal/mol*, $r_0 = 3.4$ $\mathring{A}$. The first derivative of E_{vdw} can result in the vdW atomistic force function. The relationship of the L-J pair potential and the pair force with the inter-atomistic distance is illustrated in Fig. 4.

Since the calculated responses from the MD simulation are all discrete, the definition of stress under the continuum assumption would not be
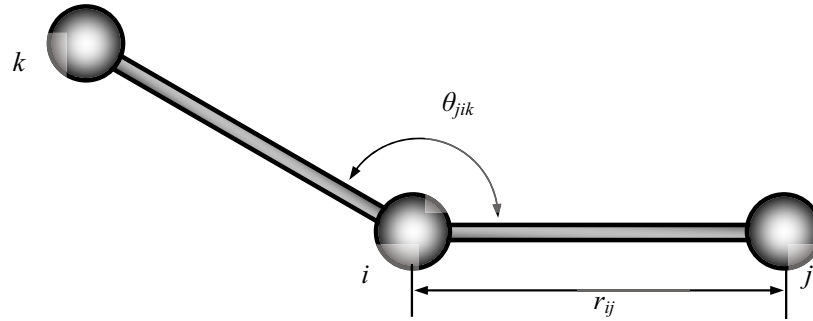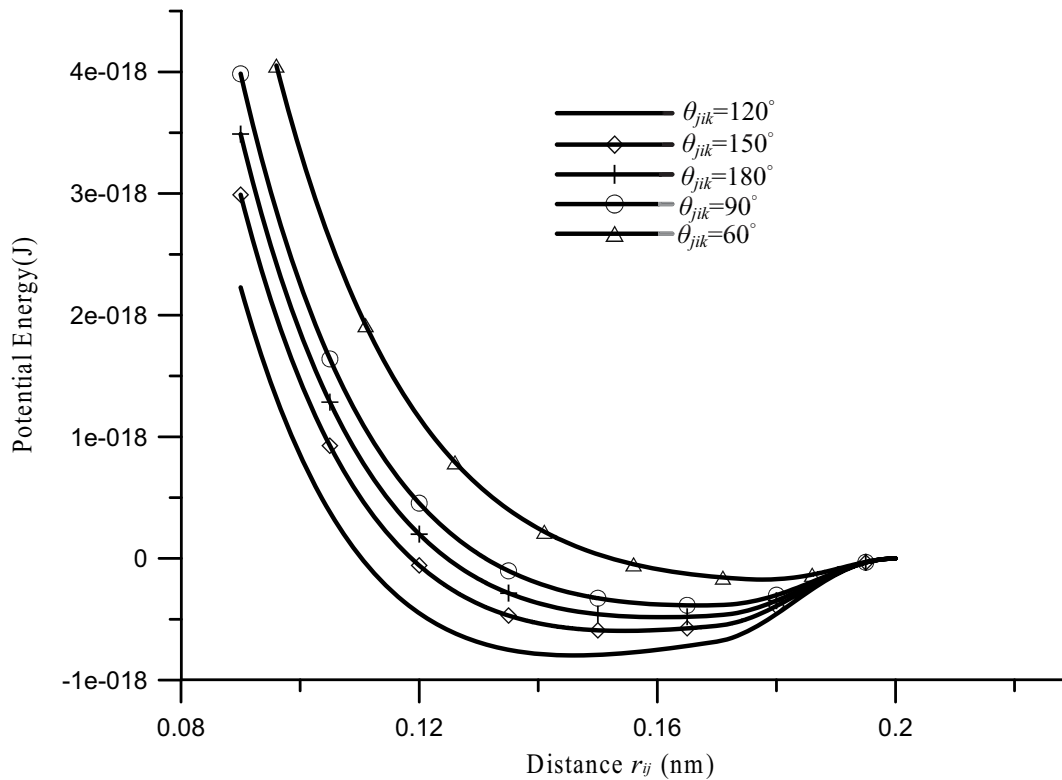
Figure 1: The geometric relation of covalent bonds

Figure 2: Tersoff-Brenner potential versus distance with different bonding angle

quite adequate for use in this study. Based on the smoothed particle hydrodynamics (SPH) technique, Shen and Atluri (2004b) addressed the concept that smoothes the discrete atomistic force field and transfers it to an equivalent continuum system. In their model, the force density $\mathbf{g}(\mathbf{r})$ at point $\mathbf{r}$ can be derived from the discrete atomistic force field by SPH method:

$$\mathbf{g}(\mathbf{r}) = \sum_i \mathbf{f}_i w(\mathbf{r} - \mathbf{r}_i, h), \tag{8}$$

where $\mathbf{f}_i$ is the force on atom i, $w(\mathbf{x}, h)$ the smooth kernel function, and $\mathbf{r}_i$ the position of atom i.

The following Gaussian function is chosen as the smooth kernel function in the study,

$$w(\mathbf{x}, h) = \frac{1}{(\sqrt{\pi}h)^d} \exp(-\frac{\mathbf{x}^2}{h^2}), \tag{9}$$

where h is the smoothing length and d the number of spatial dimensions. As h approaches to zero, the kernel function becomes a delta function. For an appropriate h, the Gaussian kernel function falls off rapidly such that only a small number of particles would contribute to the force density. At last, the relationship between the atomistic force
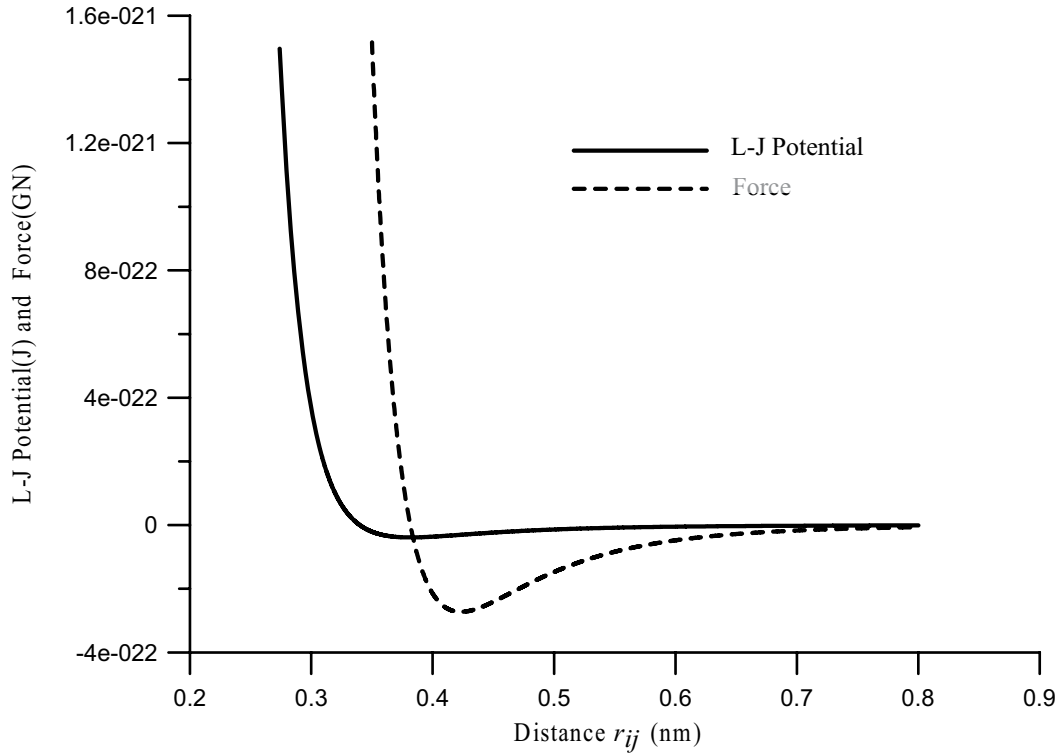
Figure 4: Lennard-Jones potential versus distance between two atoms
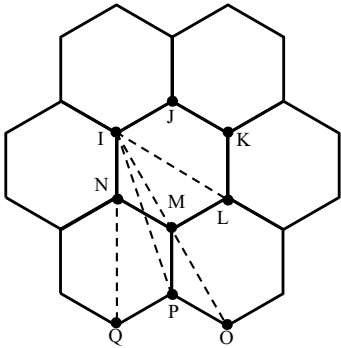

Figure 3: The valid range of vdW atomistic interactions

and stress fields is obtained by analyzing the force state of the infinitesimal parallelepiped at point **r**. With an appropriately defined smoothing length h, the Cauchy stress of the atomic level at point **r** falls into the following simple form:

$$\sigma(\mathbf{r}) = \frac{1}{2} \sum_i \sum_{j \neq i} \mathbf{r}_{ij} \otimes f_{ij} \int_0^1 w[\mathbf{r} + (\mathbf{r}_{ij}c - \mathbf{r}_j)]dc. \tag{10}$$

4   Results and Discussions

In the current investigation, three types of CNTs are performed, including the zig-zag and armchair types of S/MWCNTs, as well as the hybrid type that consists of a different chirality in the inner and outer tubes. The latter has never been addressed in literature. The mechanical properties considered include the elastic modulus, Poisson's ratio, shear modulus, and interlayer shear strengths of MWCNTs. The emphasis of the investigations is mainly placed on discussing the effect of the inlayer vdW atomistic interactions on these mechanical properties. The computed results are extensively compared against the published data obtained from numerical and experimental approaches. It should be however noted that there is a slight difference in the diameter of the zig-zag and armchair types of MWCNTs. For a zig-zag MWCNT with four layers, the associated radii from the innermost (1st layer) to the outermost (4th layer) are 0.19, 0.54, 0.89 and 1.24 (nm), while for the armchair type, the corresponding radii are 0.34, 0.68, 1.02 and 1.36 (nm).

Moreover, the radii of the two-layered or three-layered CNTs are exactly identical to those of the first two or three layers, respectively, of the four-layered CNTs.

In the calculations, strain energies are minimized for fixed strain value. The unstrained configuration is first calculated. An example of the relaxed, deformed shape of a SWCNT simply because of the surface effect and vdW interaction is shown in Fig. 5. As seen in the figure, it gives a concave configuration, in which the radius at both ends of the SWCNT is larger than that at the middle. The stress of the CNTs is further calculated generally based on the atomistic-level stress definition in Eq. (10), and the result is presented in Fig. 5. The stress distribution throughout the CNT is by no means uniform. In addition, the CNT is subjected to a compressive load, where the maximum compressive stress takes place in the middle of the CNT and the minimum at the both ends.
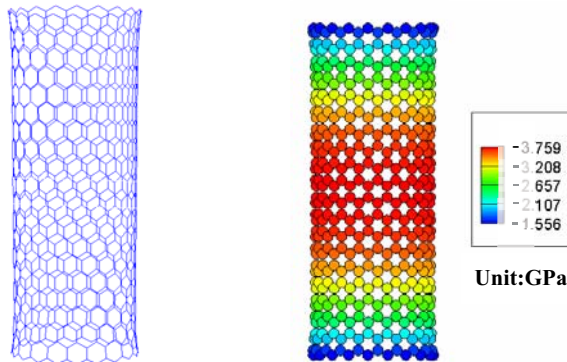

Figure 5:   The relaxation of an unstrained SWCNT and the associated compressive stress distribution

The compressive load is considered as a preload for subsequent MD simulations, in which the strain is applied to the CNTs in small time steps. The starting configuration for each energy minimization is derived from the minimized value extracted from the previous strain.

4.1   The Elastic Moduli of S/MWCNTs

The elastic moduli of the SWCNTs are first explored as a function of their radius, and the results

are shown in Fig. 6. The CNTs under the investigation are on the order of 4.06 nm long. The dependence of the inlayer vdW atomistic interactions is also presented in the same figure. It shows that the axial elastic modulus of both the zig-zag and armchair tubes increases with an increasing tube's radius, and eventually approaches a converged limit as the tube's radius becomes larger than 1.2nm. In the calculation, the armchair type of the SWCNTs turns out to be stiffer than the zig-zag type, with at most about 21% higher.

Most importantly, when the inlayer vdW atomistic interactions are not considered in the modeling, the elastic modulus of the SWCNT is altered from 704 to 1010 (GPa) for the zig-zag type and from 853 to 1021 (GPa) for the armchair type as the radius is increased from about 0.12 to 1.51 and 1.44 (nm), respectively. The limit value in the elastic moduli of these two types of SWCNTs, in which it is 1010GPa for the zig-zag type and 1021 GPa for the armchair type, are also very consistent with Li and Chou (2003a) using a molecular structural mechanics approach, Hernandez et al. (1998) using a non-orthogonal tight-binding MD simulation scheme, and Lu (1997) using an empirical model in MD simulation, in which none of them take into account of the inlayer vdW atomistic interactions either. However, the results are slightly different from those experimental results (Treacy et al., 1996; Wong et al., 1997; Krishnan et al., 1998; Salvetat et al., 1999) where the measured axial elastic modulus is in the range of 1200~1300 GPa. This might imply that there is certain insufficiency in the modeling or the empirical potential function. It is believed in the study that part of the insufficiency may be resulted from the lack of comprising the vdW atomistic interactions in the empirical potential function. Fig. 6 shows that when the inlayer vdW atomistic interactions are included, the elastic moduli of the SWCNTs correspondingly increase from 768 to 1097 (GPa) for the zig-zag tubes and from 891 to 1113 (GPa) for the armchair. The limit value is about 1097 GPa for the zig-zag tubes and 1113 GPa for the armchair, with about 9% increase as compared with those not accounting for the inlayer vdW interactions. Those results agree bet-
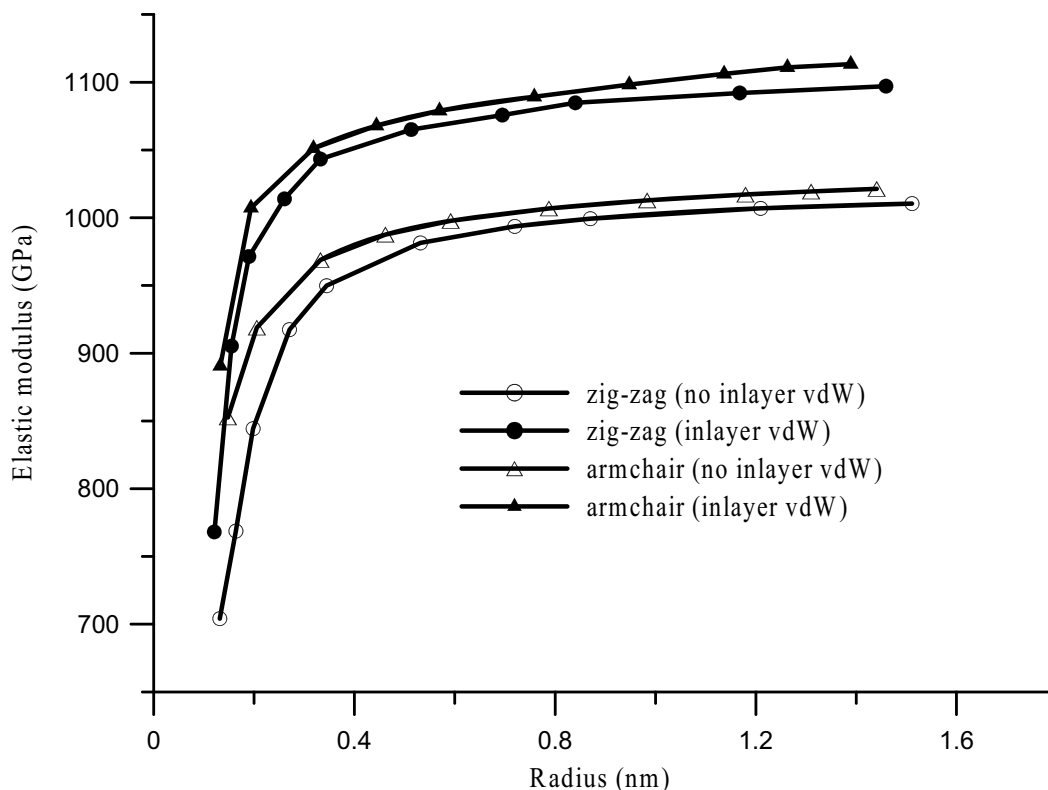
Figure 6: The elastic moduli of the SWCNTs versus nanotube's radius

ter with the existing published data (Treacy et al., 1996; Wong et al., 1997; Krishnan et al., 1998; Salvetat et al., 1999), demonstrating that the effect of the weak vdW atomistic interactions is not trivial.

As for the influences of the inlayer vdW atomistic interactions as well as the number of layers in MWCNTs on the associated modulus, Fig. 7 demonstrates that the predicted elastic moduli of the zig-zag type of the MWCNTs having 1~4 layers range from 1007 to 1019 (GPa) when the weak vdW interactions are not included, and from 1092 to1094 (GPa) when considered. Furthermore, the estimated elastic moduli of the armchair type of the MWCNTs having 1~4 layers range from 1019 to 1049 (GPa) when the weak vdW interactions are not included, and 1111~1114 (GPa) when included. In principal, the trend of the results when not accounting for the weak vdW atomistic interactions is in good agreement with Li and Chou(2003b) using a molecular structural mechanics approach and Lu et al. (1997) using MD simulation.

Few remarks can be summarized from the above results. First, when the inlayer vdW interactions are taken into account, the elastic moduli tend to be independent of the number of layers in the MWCNTs while they almost increase with an increasing number of layers when the vdW interactions are not considered. Second, the armchair type tends to be stiffer than the zig-zag one, which also agrees well with the published data (Natsuki and Endo, 2004; Meo and Rossi, 2006; Wu et al., 2006). Last, the effect of the inlayer vdW interactions could contribute up to 9% of the elastic modulus of the MWCNTs.

Fig. 8 shows the elastic moduli of the double-walled CNTs versus nanotube's radius. In addition to the zig-zag and armchair tubes, the investigation also covers the hybrid tubes. It should be noted that for the hybrid type, its outer layer is zig-zag and its inner layer armchair. Besides, the radius of these double-walled CNTs is equivalent, in which it varies from 0.19 to 1.24 (nm) for the inner layer and from 0.54 to 1.51 (nm) for the outer layer. Again, the results when considering
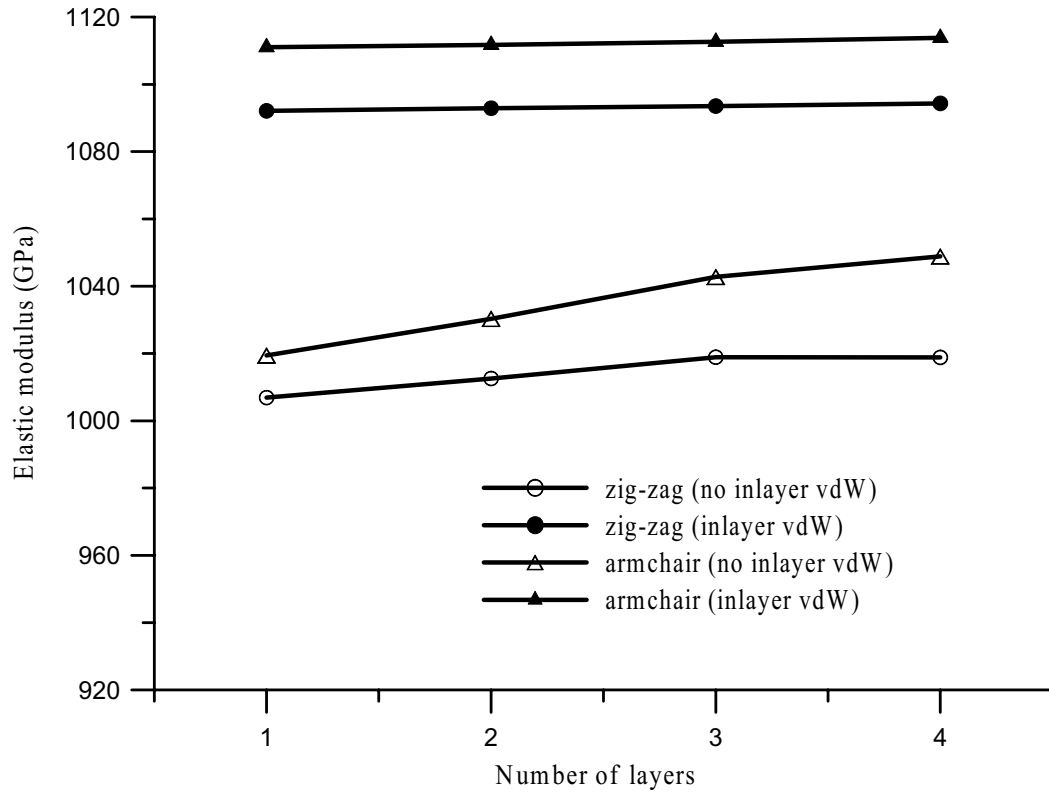
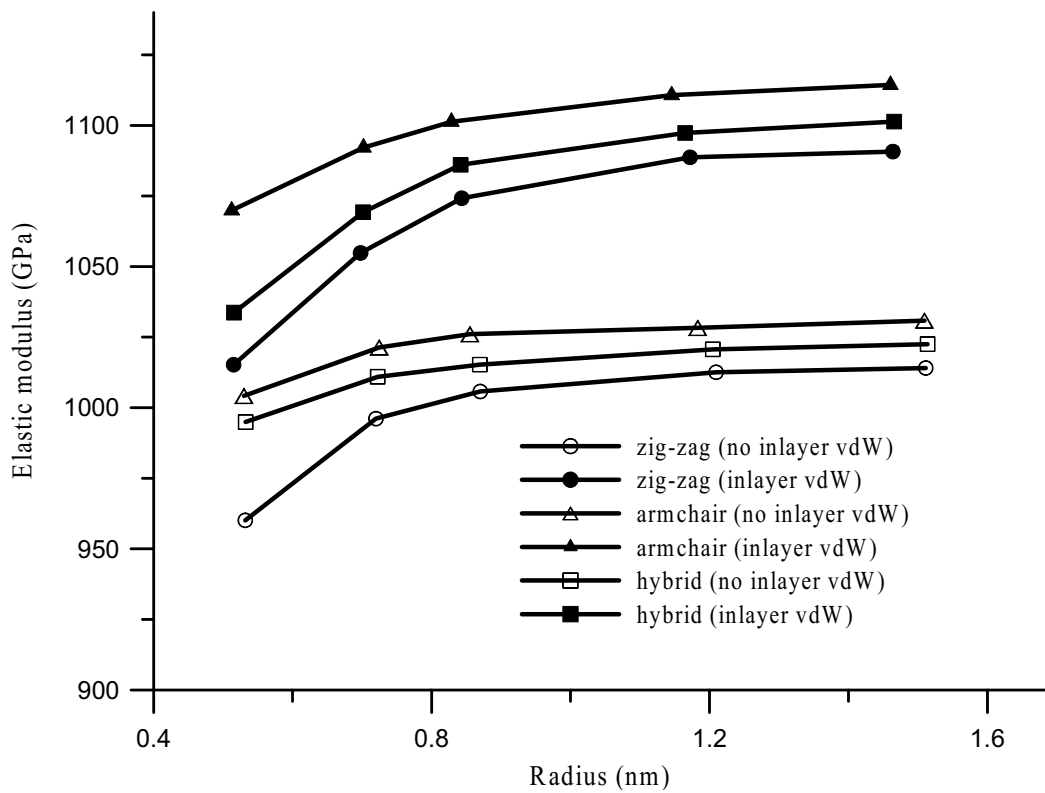Figure 7: The elastic moduli of the MWCNTs containing a different number of layers

Figure 8: The elastic moduli of the double-walled CNTs versus nanotube's outer radius

the inlayer vdW interactions surpass those when not, in spite of the chirality of the tubes. The difference can be up to 8%, implying that the inlayer vdW interactions can play a certain part in the mechanical properties, and should not be neglected in the modeling. For the double-walled CNTs, the elastic moduli converge with an increasing radius to different limits for these cases. The tendency of the results is somewhat similar to that of the SWCNTs, as shown in Fig. 6. Furthermore, it is interesting to note that the elastic moduli of the hybrid tubes are in between those of the zig-zag and armchair tubes. This might be mainly due to the specific configuration of the hybrid tubes that consist of a zig-zag outer layer and an armchair inner layer.

To examine why the inlayer vdW interactions can upgrade the elastic moduli of CNTs, the resultant forces of the S/MWCNTs when subjected to an enforced, axial elongation 0.1 $\mathring{A}$ at one side and a fixed boundary condition at the other side are presented in Table 1. It shows that the resultant forces for the cases with the inlayer vdW interactions are larger than those without. This clearly explains why the weak inlayer vdW interactions can raise the material strength of CNTs.

Subsequently, the effect of the orientation variation between the inner and outer layers in a doubled-walled CNT on its elastic modulus is investigated, in which the inner layer is rotated against the outer layer in a counterclockwise direction. Note that the chirality of these two layers is identical. Based on the specific configuration of the MWCNT shown in Fig. 9, in which the inner layer comprises 23 atoms and the outer layer 32 atoms, a cyclic, orientation mismatch of 11.25 degree can be recognized. The dependence of the orientation mismatch angle on the elastic moduli is shown in Fig. 10. It turns out that irrespective of whether there are the inlayer vdW atomistic interactions or not, the elastic moduli seem to be independent of the orientation variation between them.

4.2 The Poisson's Ratios of S/MWCNTs

The Poisson's ratios of the zig-zag and armchair types of the SWCNTs versus nanotube's radius

are presented in Fig. 11. It clearly shows that the Poisson's ratios decrease with the tube's radii increasing. In addition, the Possion's ratios of the zig-zag type of the SWCNTs tend to be larger than those of the armchair ones (Shintani and Narita, 2003; Wu et al., 2006). It is also noted that the Poisson's ratios converge to a limit as the tube's radius reaches 3nm, which are consistent with those obtained by the previous calculations (Wu et al., 2006; Xiao and Hou, 2006). Furthermore, as shown in Fig.11, the Poisson's ratios become smaller as the inlayer vdW atomistic interactions are considered. The decrease can be up to about 27% for the zig-zag type and 25% for the armchair type.

As for the dependence of the orientation mismatch between the inner and outer layers on the Poisson's ratio, the results are shown in Fig. 12. Note that the configuration of the double-walled CNT that is performed herein can be referenced to Fig. 9. Evidently, the Poisson's ratios are also independent of the orientation variation between the inner and outer layers, irrespective of with or without the inlayer vdW atomistic interactions.

Fig 13 presents the dependence of the number of layers in MWCNTs on the Poisson's ratio. Results show that the Poisson's ratios converge with the number of layers in a MWCNT regardless of the chirality of the tubes or whether the weak inlayer vdW atomistic interactions are considered or not. In addition, the weak inlayer vdW atomistic interactions considerably reduce the Poisson's ratios. Similar to the results of the SWCNTs, the Poisson's ratios of the zig-zag type of the MWCNTs are also larger than those of the armchair (Shintani and Narita, 2003; Wu et al., 2006) and rapidly converge with the number of layers to different limits, which is 0.25 for the zig-zag type and 0.23 for the armchair type. The results agree considerably well with the theoretical data calculated by molecular mechanics by Xiao and Hou (2006).

Fig. 14 reveals the Poisson's ratios of the double-walled CNTs versus nanotube's radius. The geometry of the double-walled CNTs used in the current investigation is the same as those applied in Fig. 8. It shows that irrespective of the chi-

Table 1: The resultant forces for the cases with/without the inlayer vdW interactions

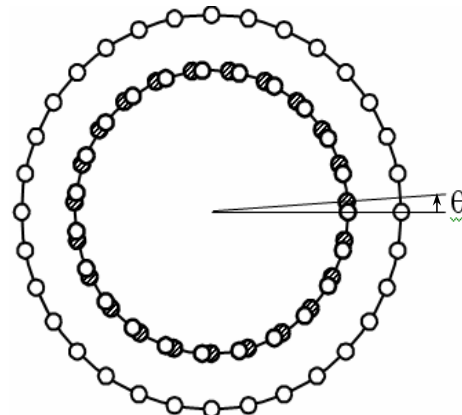| resultant forces	SWCNT	MWCNT (two layers)	MWCNT (three layers)
without inlayer vdW interactions	2.521E-09	4.257E-09	5.379E-09
with inlayer vdW interactions	3.349E-09	5.762E-09	7.146E-09

unit: Newtons

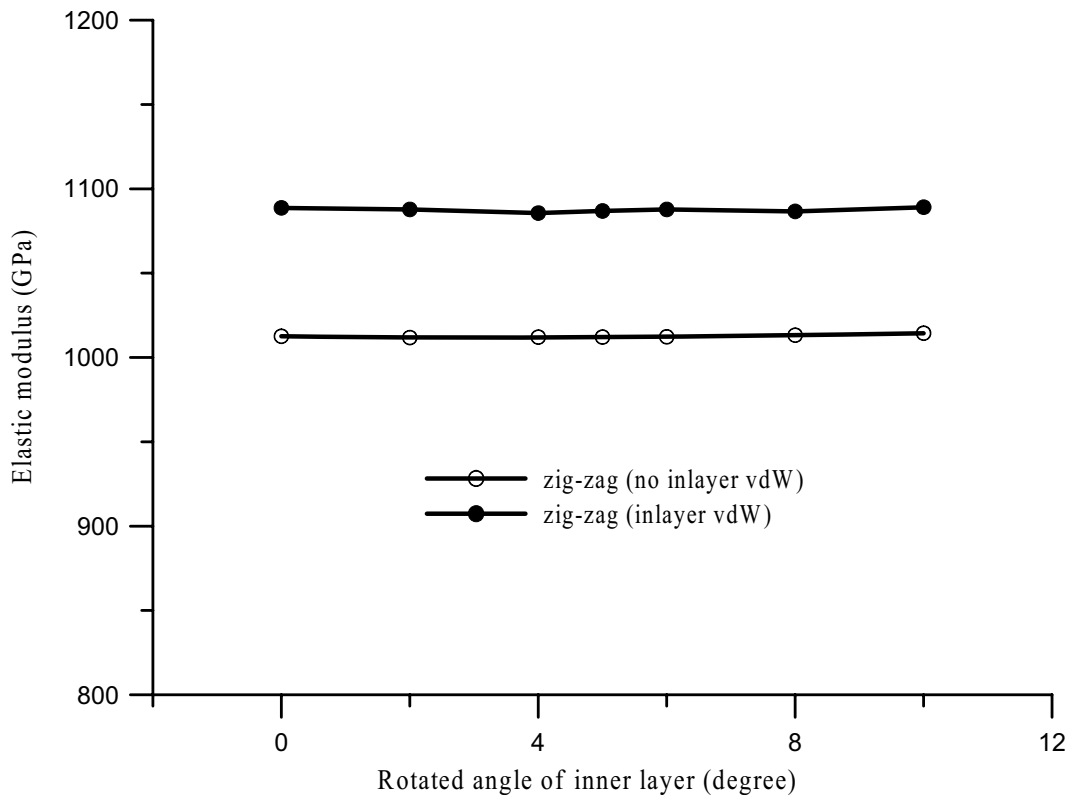Figure 9: The orientation variation between the inner/outer layers
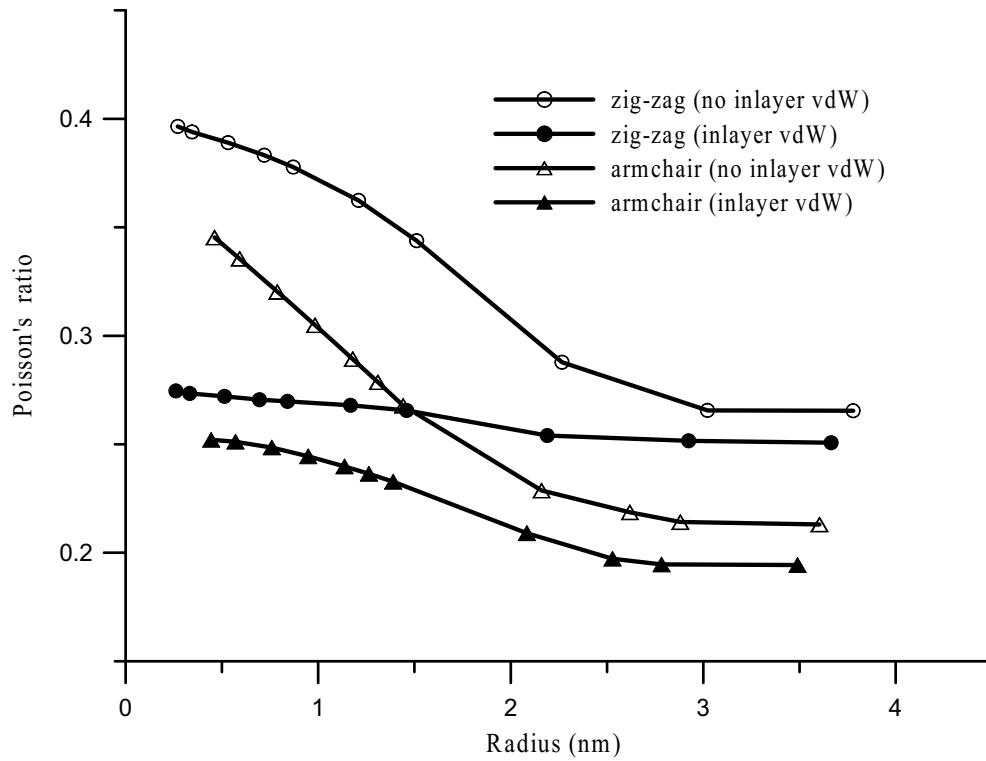

Figure 10: The elastic moduli versus the orientation variation of the inner/outer layers

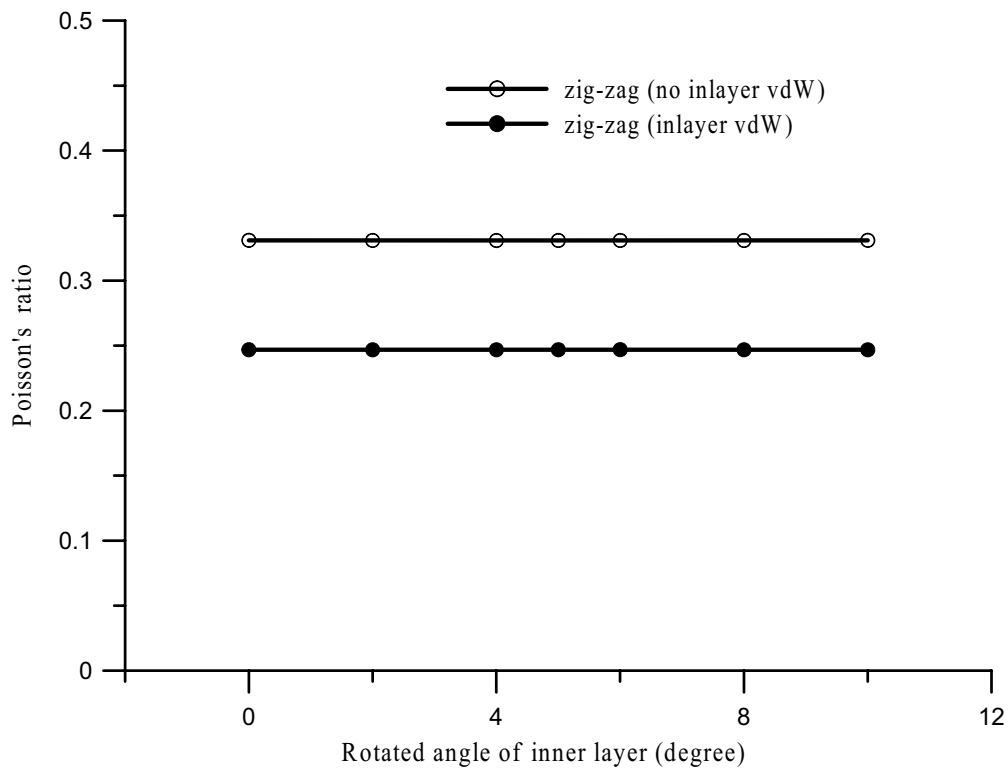Figure 11: The Poisson's ratios of the SWCNTs versus nanotube's radius

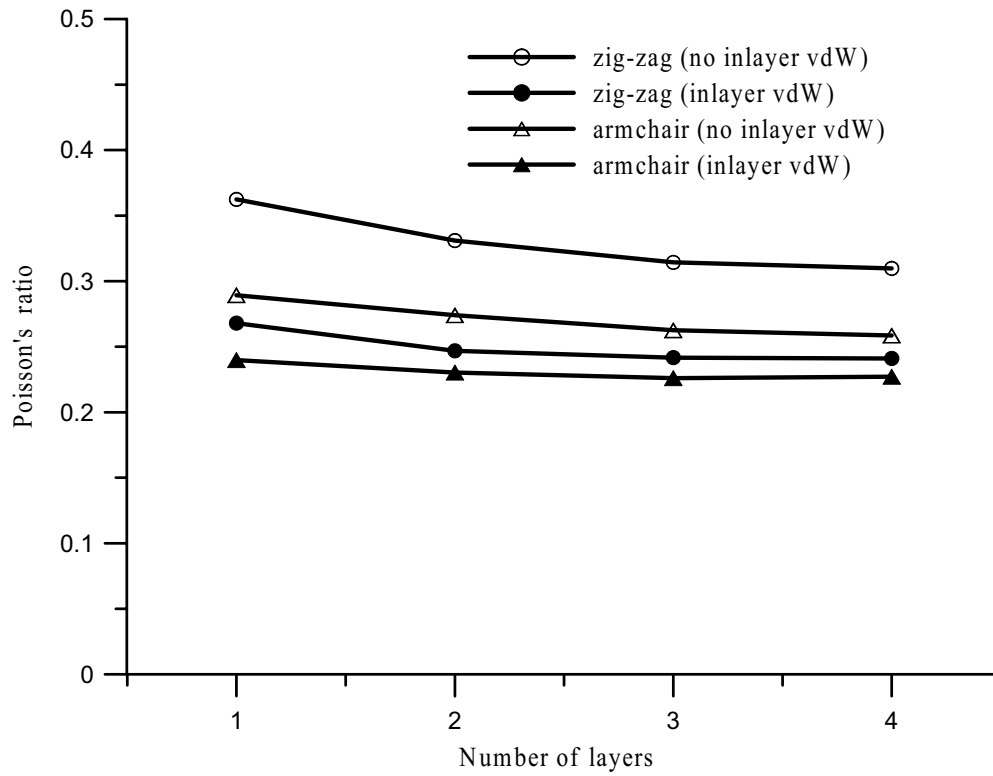Figure 12: The Poisson's ratios versus the relative orientation angles of the inner/outer layers

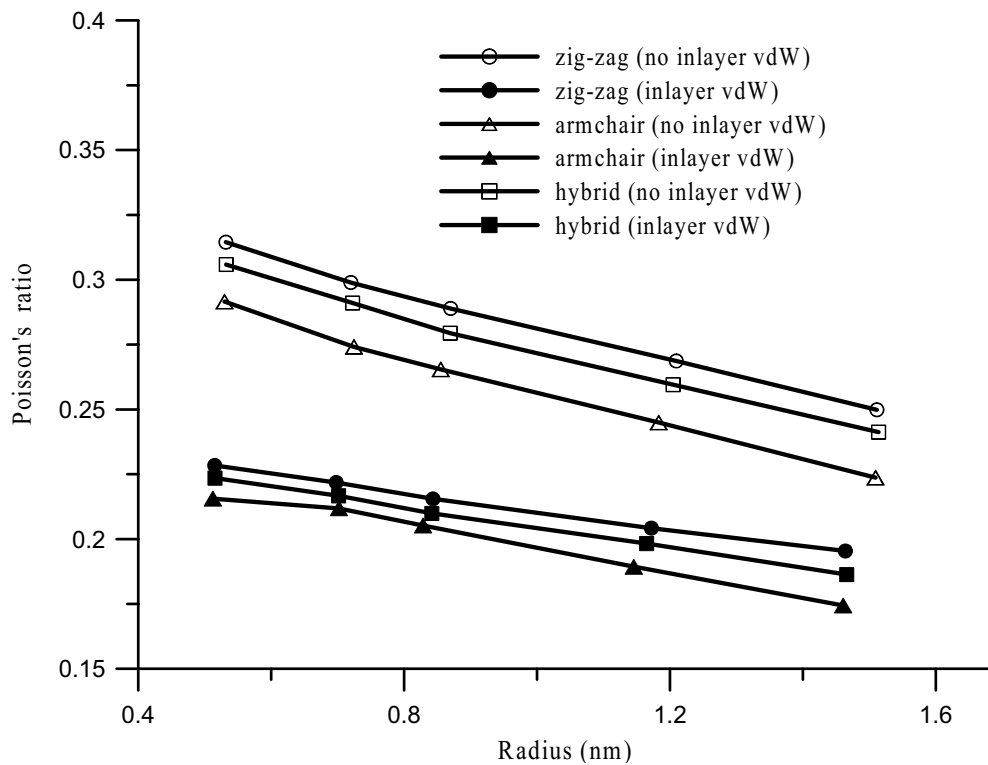Figure 13: The Poisson's ratios of the MWCNTs versus the number of layers

Figure 14: The Poisson's ratios of double-walled CNTs versus nanotube's outer radius

rality of the tubes, the Poisson's ratios with the inlayer vdW interactions are much less than those without. This again confirms that the inlayer vdW atomistic interactions can increase the material stiffness and, as a result, upgrade the transverse bending rigidity of the walls of CNTs and reduce the Poisson's ratios. The difference is about 25% for these three types of tubes, indicating that the effect of the weak inlayer vdW interactions on the Poisson's ratios is by no means "weak". Without taking the interactions into account would result in an overestimated Poisson's ratio. This explains why Lu (1997) and Li and Chou (2003a; 2003b) that did not consider the effect gave a larger Poisson's ratio than the current work. For the double-walled CNTs, the Poisson's ratios decrease with the increase of tube's radius. It is also not surprising to find that the Poisson's ratios of the hybrid tubes are in between those of the zig-zag and armchair, and the trend of which is also consistent with that of the elastic moduli of the double-walled CNTs, as shown in Fig. 8.

An example of the deformation plot of a SWCNT when subjected to 0.1 $\mathring{A}$ axial elongation is illustrated in Fig. 15. It is found that the radial deformation of the tube is less significant when the inlayer vdW interactions are involved. This might be owing to that most of the inlayer vdW atomistic interactions provide attractive forces among non-bonding atoms. As mentioned earlier, the attractive forces can shorten the axial length of the tube and enhance the associated elastic modulus. Based on the continuum mechanics, an enhanced elastic modulus would make the wall of the tube better transverse bending rigidity, thus preventing them from radial deformations and leading to a less Poisson's ratio.

4.3   The Shear Moduli of SWCNTs

The shear moduli of SWCNTs are derived by virtue of the variation of total potential energy due to the shear strain (γ). To calculate the associated total potential energy, one side of SWCNTs is imposed by a small twisting angle while fixing the other side. The shear moduli of the SWCNTs associated with the zig-zag and armchair tubes are presented in Fig. 16. Their dependence on

the inlayer vdW atomistic interactions is also presented in the same figure. It shows that the shear moduli with the inlayer vdW forces are superior to those without. Similar to the calculations of the elastic moduli, the inlayer vdW atomistic interactions can also upgrade the shear moduli of CNTs. The difference can be up to 12% for the zig-zag type and 9% for the armchair. This again indicates that the inlayer vdW interactions are not trivial. In addition, the shear moduli of the SWCNTs increase with tube's radius and approach to a convergent limit as the tube's radius exceeds 0.8 nm. Furthermore, the armchair SWCNTs turn out to be stiffer than the zig-zag when the radius of tubes exceeds 0.4 nm. Basically, the results are in agreement with the published data from force-constant model calculations (Popov et al., 2000) and molecular mechanics (Xiao et al, 2005).

4.4   The Interlayer Shear Force/Strength of MWCNTs

The interactions among atoms in neighboring layers of a MWCNT are usually modeled by the vdW atomistic forces (Li and Chou, 2003b), which are generally described by the L-J potential. As a result of the interlayer interactions, the individual layers can be connected together to form a MWCNT. To understand the interlayer non-bonding shear strength, the interlayer shear force in a doubled-walled CNT is explored. The double-walled CNT under the investigation consists of an inner and outer layer of 0.19 nm and 0.54 nm in radius, respectively, and 4.06 nm in length. Three different types of the double-walled CNT are investigated herein, including the zig-zag, armchair and hybrid. In the MD calculations, the inner layer is pulled out with a length L against the outer layer, the left end of which is fixed, as shown in Fig. 17.

The resultant shear forces of those three types of the double-walled CNTs versus the pull-out length (L) of the inner layer are presented in Fig. 18. In the figure, the effect of the inlayer vdW atomistic interactions on the interlayer shear forces is also drawn. As can be seen in the figure, the interlayer vdW atomistic interactions are mainly attractive forces during the pulling pro-
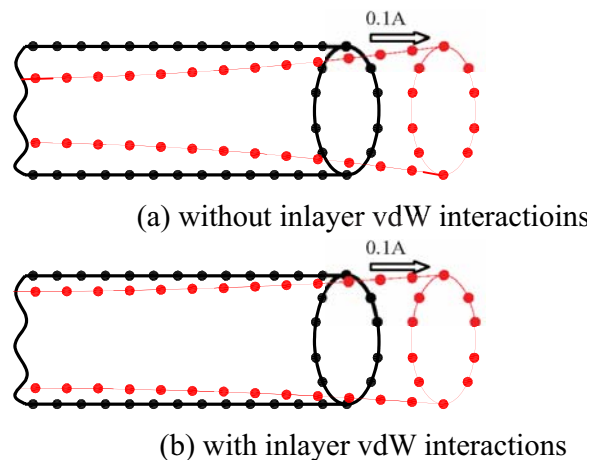
(a) without inlayer vdW interactioins

(b) with inlayer vdW interactions

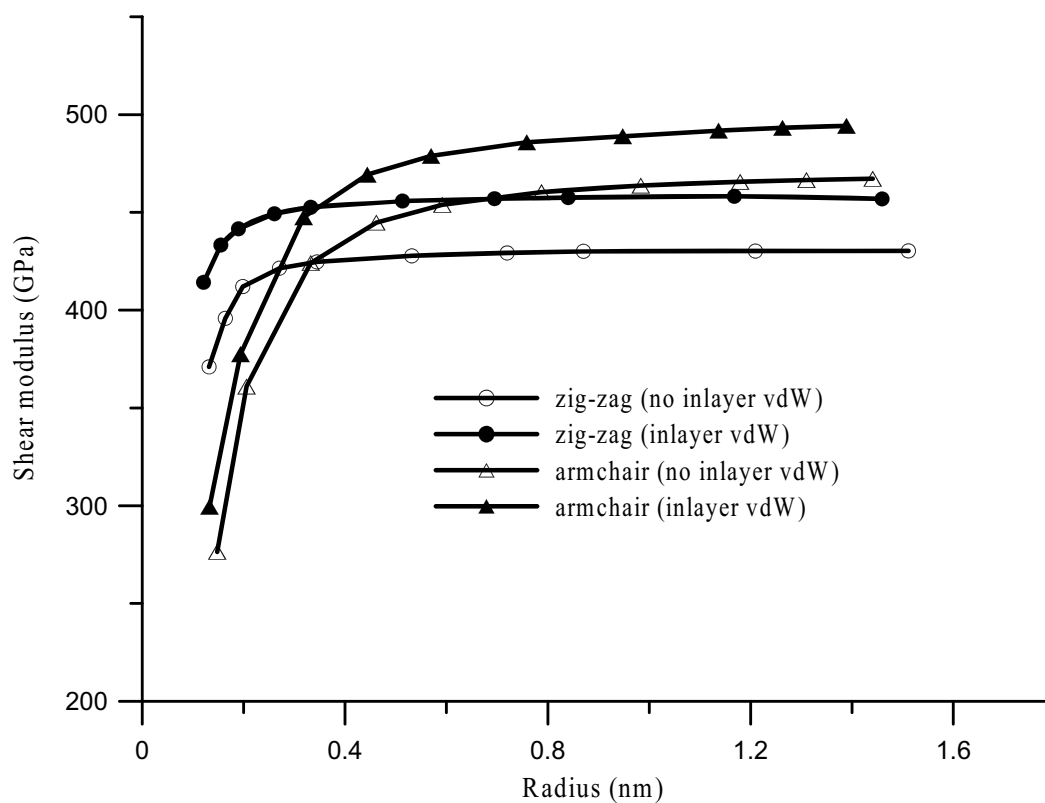Figure 15: The configuration of the SWCNT before/after applying 0.1 Å axial deformation

Figure 16: The shear moduli of SWCNTs versus nanotube's radius

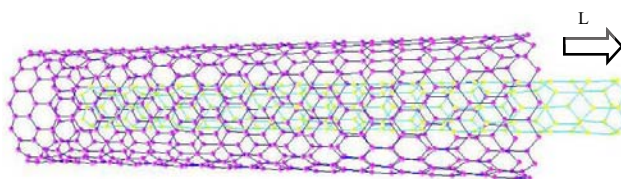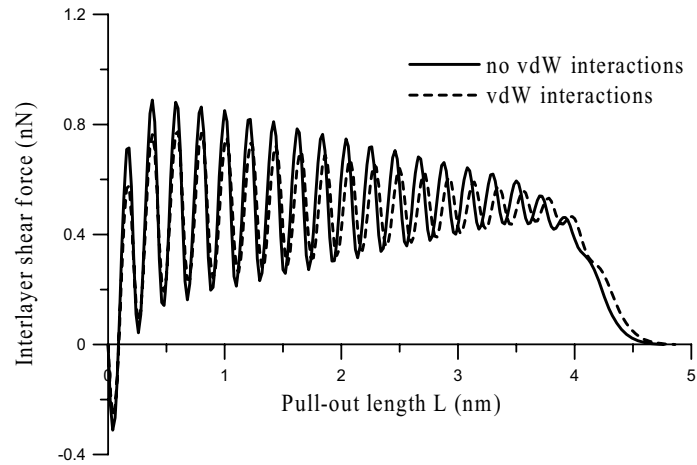
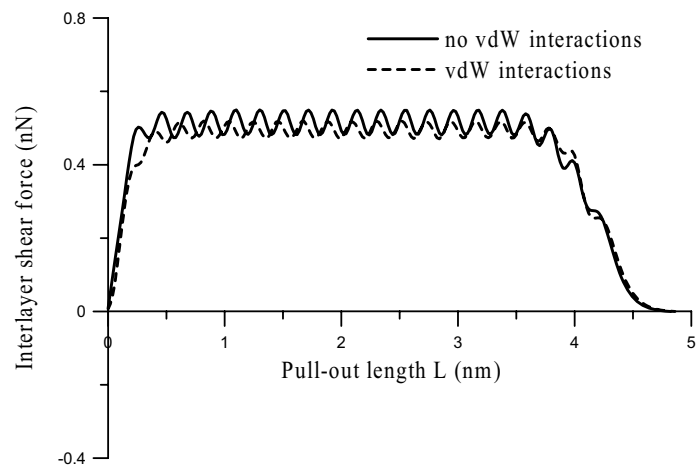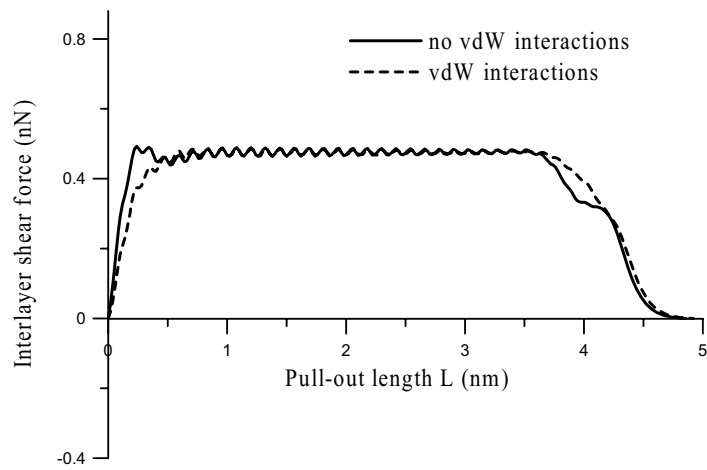
Figure 17: Pullout the inner layer of a double-walled CNT

(a) The zig-zag type

(b)The armchair type

(c)The hybrid type

Figure 18: The interlayer shear force of the double-walled CNT versus the pull-out length

cess. It is observed that there is a certain extent of fluctuation in the interlayer shear forces. The amplitude of the fluctuation for the zig-zag type is most distinct, followed by the hybrid type and the armchair type. Furthermore, the results with the inlayer vdW interactions tend to hold smaller amplitudes than those without, which in specific, would cause a drop of about 13% for the zig-zag type, 5.5% for the hybrid one and 1% for the armchair one. It should be noted that the maximum interlayer shear force in the figure can be considered as the interlayer shear strength of the double-walled CNTs, which implies that an external force larger than that is required to separate these two layers.

Fig. 19 shows the averaged interlayer shear forces associated with those three types. Essentially, they increase with the pull-out length before reaching a maximum value. The maximum limit is basically attained when the pull-out length of the inner layer is about 0.8 nm. Subsequently, they maintain the value throughout the most of the rest of the pulling process, and eventually decrease to a zero value when both layers are completely separated. It is clearly shown that under the same length of the double-walled CNTs, as seen in Fig. 18, the zig-zag type gives the largest interlayer shear strength (0.889 nano-Newton, nN), followed by the hybrid (0.550 nN) and the armchair (0.493 nN). This again proves that the mechanical properties of the hybrid type are likely in between the zig-zag and armchair types. The results in Fig. 19 can be explained in the following by means of Fig. 20. The interlayer shear force of a MWCNT can be mainly attributed to the vdW interactions of the atoms in the inner layer beyond the overlapping region of these two walls with those in the outer layer. As the pulling process begins, atom A starts to move rightward away from the atom K, resulting in an attractive pair interaction. The attractive pair interaction increases as atom A is further moved rightward away from atom K and as more atoms in the inner layer go beyond the end side of the outer layer. This indicates why the averaged interlayer shear force would increase with the pull-out length in the beginning. It can be observed that there ex-

ists a convergent limit in the averaged interlayer shear force. This is mainly because there is a specific effective interaction range (0.8 nm) for the interlayer vdW force, as seen in Fig. 4. The pair interactions would reduce to zero for atom pairs that are over the range; as a result, the vdW interactions become ineffective even though more and more atoms in the inner layer are participating in the interactions. Fig. 4 and Fig. 20 demonstrate the effective pair interaction range for the interlayer vdW force.

On the other hand, the atomistic configuration of the CNTs is primarily attributed to the fluctuation of the interlayer shear forces in Fig. 18. It is clear that each atom in the inner layer would be subjected to two sources of attractive pair forces, one from the atoms in the outer layer at its left-hand side, and the other from those at the right-hand side. Basically, the pair interactions of the atom with the closer neighboring atoms in the outer layer are the main contribution to the net force on any of these atoms, which would be the sum of these attractive forces. For those atoms in the inner layer that are within the overlapping region of the tubes but a certain distance away from those two end sides of the outer layer, e.g. atom D, C and B, the net force on any of these atoms is null when the atoms at the inner and outer layers are exactly aligned together, i.e., where atom B is aligned to atom L, atom C to atom M etc., as shown in Fig. 20. This is because these two resultant attractive forces have the same magnitude but in opposite direction. At present, the only forces that keep the inner layer from moving rightward is the vdW interactions of the pair atoms in the inner layer beyond the overlapping zone of these two walls. When the inner layer is slightly moved rightward, the system becomes a state of non-equilibrium. These atoms would experience a larger resultant attractive force from their left-hand side than that of their right-hand side, resulting in a net force that operates in the opposite direction against the initial loading, and thus preventing the inner layer from moving rightward.

As these atoms, e.g., atom D, attain the position midway between their counterparts, e.g., atom N
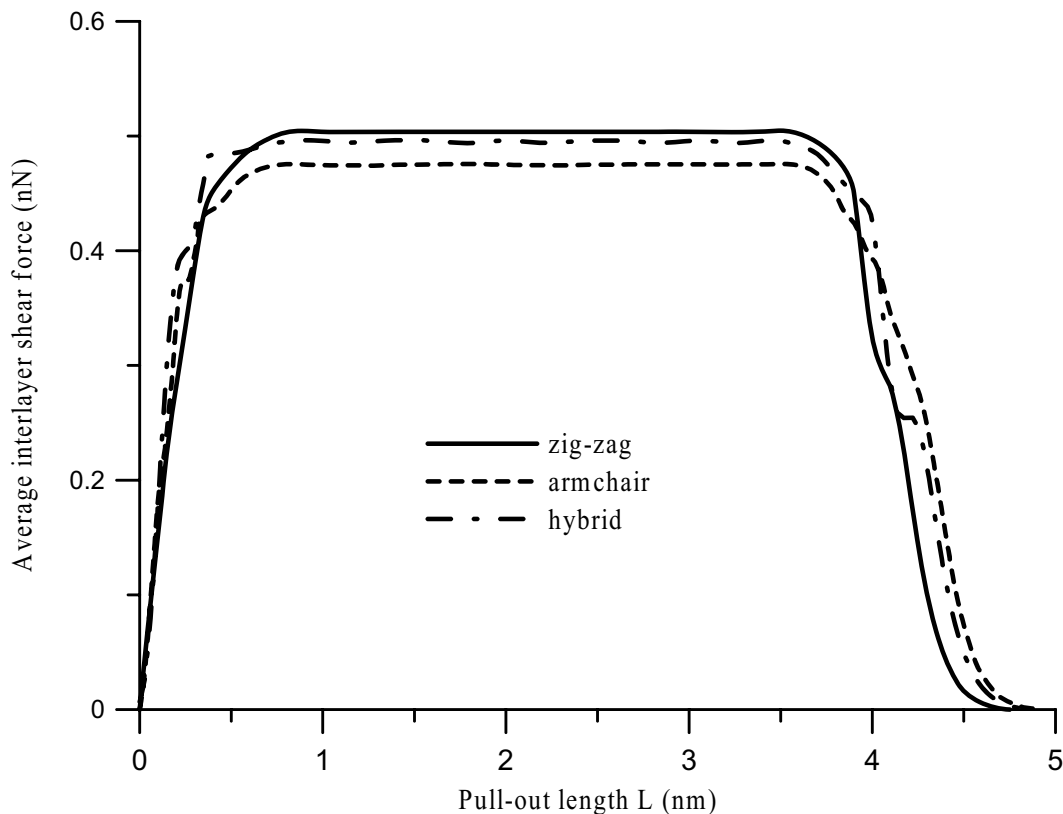
Figure 19: The averaged interlayer shear force of the three types of the double-walled CNTs
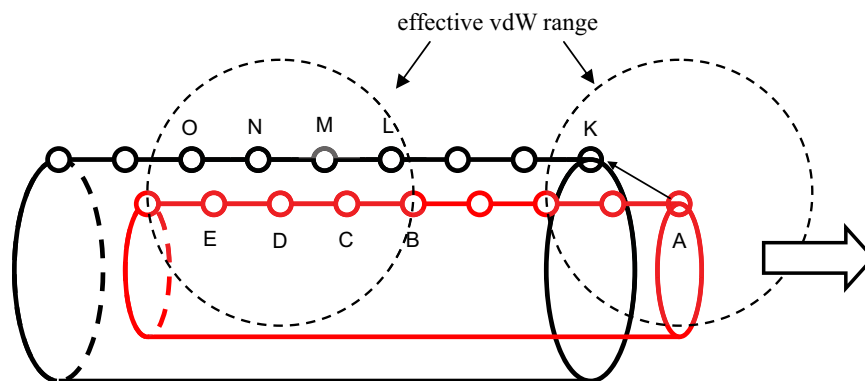

Figure 20: The atomistic arrangement and the pair interactions in a CNT

and M, its pair interactions with the atoms in the outer layer at its left- and right-hand sides would resume equilibrium, and the net force on each of the atoms becomes null. As the inner layer is further pulled out, where, e.g., atom D is approaching to atom M, the resultant attractive force at their right-hand side would be larger than that of the left-hand side. This leads to a net force that operates in the same direction as the initial load-

ing, thus facilitating the rightward movement of the inner layer. Furthermore, when the atoms at the inner and outer layers are again aligned together, i.e., where atom E is aligned to atom N, atom D to atom M and atom C to atom L etc., the net force on these atoms would again resume null. In other words, it would consist of the same interlayer shear force as the initial, strained state. In brief, this completes a cycle of the fluctuation.

The process continues until there is barely any overlapping region between the inner and outer layers. The sum of the net force on each of these atoms establishes the resultant net force, which fluctuates with the pull-out length because of the repeated atomistic arrangement of CNTs. The amplitude of the fluctuation would be reduced as the atoms that are located within the overlapping section of the tubes become less. This can be clearly observed in Fig. 18(a), where the amplitude of the fluctuation decreases with the pull-out length. Besides, the magnitude of the amplitude is also dependent of the atomistic configuration, as can be also confirmed in Fig. 18 (a)-(c). The fluctuations together with the averaged interlayer shear forces shown in Fig. 19 constitute the total interlayer shear forces.

The influence of the tube's radius on the interlayer shear force and strength is analyzed here. A zig-zag type of the double-walled CNTs with three different sets of radius is considered, including 0.19/0.54 (nm) (the radius of the inner/outer layers), 0.54/0.89 (nm) and 0.89/1.24 (nm). It is clear that the interlayer shear strength increases with radius, in which it is 0.615 nN for the case of "0.19/0.54 (nm)", 0.774 nN for "0.54/ 0.89 (nm)" and 0.943 nN for "0.89/1.24(nm)". Specifically, the increase of the interlayer shear strength is about 26% and 53% when the radius of the double-walled CNTs is correspondingly enlarged from 0.19/0.54 (nm) to 0.54/ 0.89 (nm) and 0.89/1.24 (nm). In addition, the associated amplitude of the fluctuations grows with the radius. This could be due to that an increasing radius would accordingly comprise a greater number of atoms in the cross section of the CNTs, thus resulting in more significant pair interactions at the neighboring layers. Moreover, the peaks of these fluctuations remain unshifted even though the corresponding radius of the CNTs is different.

The effect of the interlayer spacing on the interlayer shear strength is also explored. It is achieved by way of fixing the innermost radius while increasing the outermost radius. Three sets of interlayer spacing are considered in the investigation, including 0.34, 0.50 and 0.70 (nm). It turns out that the interlayer shear force and strength and the associated amplitude of the fluctuations decrease with the increase of interlayer spacing because of the growth of the interlayer distance between neighboring layers. The shear strength for the interlayer spacing of 0.50 nm and 0.70 nm is 0.361 and 0.026 (nN), respectively, and there are about 53% and 97% less in comparison with the case of 0.34 nm. This implies that those MWCNTs with an interlayer spacing larger than 0.34 nm may not be detected in the real natural world due to its weak interlayer shear strength. This may explain why the interlayer spacing of MWCNTs all maintains a value of 0.34 nm.

The dependence of the length of MWCNTs on the interlayer shear force and strength is also presented herein. The double-walled CNTs considered in the investigation are associated with a different length, including 1.96, 4.06 and 6.16 (nm). Results show that the longer the length of the MWCNTs, the more the number of atoms in the CNTs and thus, the larger the amplitude of the fluctuation and the interlayer shear strength. However, the averaged interlayer shear forces associated with these three double-walled CNTs are considerably comparable due to that there are an equivalent number of atoms in the cross section of the CNTs.

5 Conclusions

The effect of the inlayer vdW atomistic interactions on the fundamental mechanical properties of various S/MWCNTs with different dimensions and geometry configurations has been successfully estimated using MD simulations. The mechanical properties of CNTs under investigation include elastic modulus, shear modulus, Poisson's ratio and interlayer shear strength. The axial orientation mismatch between the inner and outer layers of MWCNTs on the associated mechanical properties and the interlayer shear force of MWCNTs are also analyzed extensively.

Some concluding remarks can be drawn:

1) The computed results that account for the inlayer vdW atomistic interactions show that the elastic moduli, shear moduli and interlayer shear strength of those S/MWCNTs can have

up to about 9%, 12% and 13% increase, respectively, while the Poisson's ratios 27% decrease. Apparently, the effect of the inlayer vdW interactions plays a significant role on the calculation of the mechanical properties of CNTs. Most importantly, the results with the inlayer vdW interactions could be in more agreement with the experimental data.

2) The axial orientation mismatch effect between the inner and outer layers of MWCNT on the mechanical properties of CNTs can be ignored.

3) The mechanical properties of the hybrid MWCNTs are midway between the zig-zag and armchair MWCNTs.

4) The atomistic arrangement and the number of atoms in a cross section of MWCNTs would determine the magnitude of the averaged interlayer shear force while the length of MWCNTs would govern the magnitude of the fluctuation of the interlayer shear force. That is, these three parameters manage the interlayer shear strength of MWCNTs.

The present MD simulations can be further extended to investigate the stress-strain relations and the fracture behaviors of S/MWCNTs. Those will be presented in a subsequent report.

Reference

Abell, G. C. (1985): Empirical chemical pseudopotential theory of molecular and metallic bonding. *Physical Review B*, 31: 6184-6196.

Battezzatti, L.; Pisani, C.; Ricca, F. (1975): Equilibrium conformation and surface motion of hydrocarbon molecules physisorbed on graphite. *J. Chem. Soc.*, 71: 1629-1639.

Brenner, D. W. (1990): Empirical Potential for Hydrocarbons for Use in Simulating the Chemical Vapor Deposition of Diamond Films. *Physical Review B*, 42: 9458-9471.

Burkert, U.; Allinger, N. L. (1982): *Molecular Mechanics*. American Chemical Society. (Washington, D.C.)

Chang, T. C.; Gao, H. J. (2003): Size-dependent elastic properties of a single-walled carbon nanotube via a molecular mechanics model. *Journal of the Mechanics and Physics of Solids* 51: 1059-1074.

Chelikowsky, J. R. (1992): Formation of C_{60} clusters via Langevin molecular dynamics. *Physical Review B*, 45: 12062-12070.

Falvo, M. R.; Clary, G. J.; Taylor II, R. M.; Vhi, V.; Brooks Jr., F. P.; Washburn, S.; Suerfine, R. (1997): Bending and buckling of carbon nanotubes under large strain. *Nature*, 389: 582-584.

Gao, G. H.; Cagin, T.; Goddard III, W. A. (1998): Energetics, structure, mechanical and vibrational properties of single-walled carbon nanotubes. *Nanotechnology*, 9: 184-191.

Guo, W.; Gao, H. (2005): Optimized Bearing and Interlayer Friction in Multiwalled Carbon Nanotubes. *CMES: Computer Modeling in Engineering and Sciences*, 7: 19-34.

Heggie, M. I. (1991): Semiclassical interatomic potential for carbon and its application to the self-interstitial in graphite. *Journal of Physics: Condensed Matter*, 3: 3065-3079.

Hernandez, E.; Goze, C.; Bernier, P.; Rubio, A. (1998): Elastic properties of C and $B_xC_yN_z$ composite nanotubes. *Physical Review Letters*, 80: 4502-4505.

Huntington, H. B. (1958): *Solid State Phys.*, 7: 213-351.

Iijima, S. (1991): Helical microtubules of graphitic carbon. *Nature*, 354: 56-58.

Khor, K. E.; Das Sarma, S. (1988): Proposed universal interatomic potential for elemental tetrahedrally bonded semiconductors. *Physical Review B*, 38: 3318-3322.

Kiang, C. H.; Endo. M.; Ajayan, P. M.; Dresselhaus, G.; Dresslhaus, M. S. (1998): Size Effect in Carbon Nanotubes. *Physical Review Let-*

ter, 81: 1869-1872.

Krishnan, A.; Dujardin, E.; Ebbesen, T. W.; Yianilos, P. N.; Treacy, M. M. J. (1998): Young's modulus of single-walled nanotubes. *Physical Review B*, 58: 14013-14019.

Lennard-Jones, J. E. (1924): The Determination of Molecular Fields. I. From the Variation of the Viscosity of a Gas with Temperature. *Proceedings of Royal Society*, (London) 106A: 441.

Li, C. Y.; Chou, T. W. (2003a): "Elastic moduli of multi-walled carbon nanotubes and the effect of van der Waals forces. *Composite Science and Technology*, 63: 1517-1524.

Li, C. Y.; Chou, T. W. (2003b): A structural mechanics approach for the analysis of carbon nanotubes. *International Journal of Solid and Structures*, 40: 2487-2499.

Lier, G. V.; Alsenoy, C. V.; Doran, V. V.; Geerlings, P. (2000): Ab intitio study of the elastic properties of single-walled carbon nanotubes and grapheme. *Chemical Physics Letters*, 326: 181-185.

Ling, X.; Atluri, S. N. (2006): A lattice-based cell model for calculating thermal capacity and expansion of single wall carbon nanotubes. *CMES: Computer Modeling in Engineering and Sciences*, 14: 91-100.

Lourie, O; Wagner, H. D. (1998): Evaluation of Young's modulus of carbon nanotubes by micro-Raman spectroscopy. *Journal of Materials Research*, 13: 2418-2422.

Lu, J. P. (1997): Elastic properties of carbon nanotubes and nanoropes. *Physical Review Letters*, 79: 1297-1300.

Maiti, A. (2002): Select Applications of Carbon Nanotubes: Field-Emission Devices and Electromechanical Sensors. *CMES: Computer Modeling in Engineering and Sciences*, 5: 589-600.

Maruyama, S. (2000): Molecular Dynamics Method for Microscale Heat Transfer. *Advances in Numerical Heat Transfer*, 2: 189-226.

Meo, M; Rossi, M. (2006): Prediction of Young's modulus of single wall carbon nanotubes by molecular-mechanics based finite element modeling. *Composites Science and Technology*, 66:

1597-1605.

Nasdala, L.; Ernst, G.; Lengnick, M.; Rothert, H. (2005): Finite Element Analysis of Carbon Nanotubes with Stone-Wales Defects. *CMES: Computer Modeling in Engineering and Sciences*, 7: 293-304.

Natsuki, T.; Endo, M. (2004): Stress simulation of carbon nanotubes in tension and compression. *Carbon*, 42: 2147-2151.

Nordlund, K.; Keinonen, J; Mattila, T. (1996): Formation of Ion Irradiation Induced Small-Scale Defects on Graphite Surfaces. *Physical Review Letters*, 77: 699-702.

Odegard, G. M.; Gates, T. S.; Nicholson, L. M.; Wise, K. E. (2002): Equivalent-continuum modeling of nano-structured materials. *Composites Science and Technology*, 62: 1869-1880.

Poncharal, P; Wang, Z. L.; Ugarte, D.; de Heer Popov, W. A. (1999): Electrostatic Deflections and Electromechanical Resonances of Carbon Nanotubes. *Science*, 283: 1513-1516.

Popov, V. N.; Van Doren, V. E.; Balkanski, M. (2000): Elastic properties of single-walled carbon nanotubes. *Physical Review B*, 61: 3078-3084.

Qian, D.; Liu, W. K.; Ruoff, R. S. (2001): Mechanics of C_{60} in Nanotubes. *Journal of Physical Chemistry B*, 105: 10753-10758.

Rappe, A. K.; Casewit, C. J. (1997): *Molecular Mechanics across chemistry*. University Science Books.

Salvetat, J. P.; Bonard, J. M.; Thomson, A. J.; Kulik, A. J.; Forro, L.; Benoit, W.; Zuppiroli, L. (1999): Mechanical properties of carbon nanotubes. *Applied Physics A*, 69: 255-260.

Shen, S.; Atluri S. N. (2004a): Computational Nano-mechanics and Multi-scale Simulation. *CMC: Computers, Materials & Continua*, 1: 59-90.

Shen, S.; Atluri S. N. (2004b): Atomic-level Stress Calculation and Continuum-Molecular System Equivalence. *CMES: Computer Modeling in Engineering and Sciences*, 6: 91-104.

Shintani, K.; Narita, T. (2003): Atomistic study of strain dependence of Poisson's ratio of single-walled carbon nanotubes. *Surface Science*, 532-

535: 862-868.

Stillinger, F. H.; Weber, T. A. (1985): Computer Simulation of Local Order in Condensed Phase of Silicon. *Physical Review B*, 31: 5262-5271.

Tersoff, J. (1988): New Empirical Approach for the Structure and Energy of Covalent Systems. *Physical Review B*, 37: 6991-7000.

Treacy, M. M. J.; Ebbesen, T. W.; Gibson, J. M. (1996): Exceptionally high Young's modulus observed for individual carbon nanotubes. *Nature*, 381: 678-680.

Wang, Y.; Tománek, D.; Bertsch G. F. (1991): Stiffness of a solid composed of C_{60} clusters. *Physical Review B*, 44: 6562-6565.

Wei, C.; Srivastava, D.; Cho, K. (2002): Molecular Dynamics Study of Temperature Dependent Plastic Collapse of Carbon Nanotubes under Axial Compression. *CMES: Computer Modeling in Engineering and Sciences*, 3: 255-262.

Xiao, J. R.; Gama, B. A.; Gillespie Jr, J. W. (2005): An analytical molecular structural mechanics model for the mechanical properties of carbon nanotubes. *International Journal of Solid and Structures*, 42: 3075-3092.

Xiao, S.; Hou, W. (2006): Studies of Size Effects on Carbon Nanotubes' Mechanical Properties by Using Different Potential Functions. *Fullenrenes, Nanotubes and Carbon Nanostructures*, 14: 9-16.

Wiberg, K. B. (1965): A Scheme for Strain Energy Minimization. Application to the Cycloalkanes. *Journal of the American Chemical Society*, 87: 1070-1078.

Xie, G. Q.; Long, S. Y. (2006): Elastic Vibration Behaviors of Carbon Nanotubes Based on Micropolar Mechanics. *CMC: Computers, Materials & Continua*, 4: 11-20.

Wong, E. W.; Sheehan, P. E.; Lieber, C. M. (1997): Nanobeam Mechanics: Elasticity, Strength, and Toughness of Nanorods and Nanotubes. *Science*, 277: 1971-1975.

Wu, Y.; Zhang, X.; Leung, A. Y. T.; Zhong, W. (2006): An energy-equivalent model on studying the mechanical properties of single-walled carbon nanotubes. *Thin-Walled Structures*, 44: 667-676.

Yu, M.; Lourie, O.; Dyer, M.; Moloni, K.;

Kelly, T.; Ruoff, R. (2000): Strength and breaking mechanism of multiwalled carbon nanotubes under tensile load. *Science*, 287: 637-640.